

This article was downloaded by:[University of Colorado Libraries]
[University of Colorado Libraries]

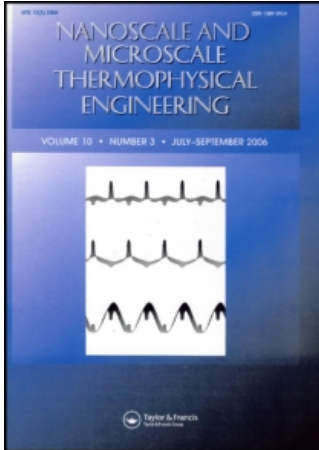
On: 4 June 2007

Access Details: [subscription number 750568220]

Publisher: Taylor & Francis

Informa Ltd Registered in England and Wales Registered Number: 1072954

Registered office: Mortimer House, 37-41 Mortimer Street, London W1T 3JH, UK



Nanoscale and Microscale Thermophysical Engineering

Publication details, including instructions for authors and subscription information:

<http://www.informaworld.com/smpp/title~content=t713774103>

A Unified Velocity Model for Digital Microfluidics

To cite this Article: Baird, E.S. and Mohseni, K. , 'A Unified Velocity Model for Digital Microfluidics', Nanoscale and Microscale Thermophysical Engineering, 11:1, 109 - 120

To link to this article: DOI: 10.1080/15567260701337514

URL: <http://dx.doi.org/10.1080/15567260701337514>

PLEASE SCROLL DOWN FOR ARTICLE

Full terms and conditions of use: <http://www.informaworld.com/terms-and-conditions-of-access.pdf>

This article maybe used for research, teaching and private study purposes. Any substantial or systematic reproduction, re-distribution, re-selling, loan or sub-licensing, systematic supply or distribution in any form to anyone is expressly forbidden.

The publisher does not give any warranty express or implied or make any representation that the contents will be complete or accurate or up to date. The accuracy of any instructions, formulae and drug doses should be independently verified with primary sources. The publisher shall not be liable for any loss, actions, claims, proceedings, demand or costs or damages whatsoever or howsoever caused arising directly or indirectly in connection with or arising out of the use of this material.

© Taylor and Francis 2007

A UNIFIED VELOCITY MODEL FOR DIGITAL MICROFLUIDICS

E.S. Baird and K. Mohseni

Aerospace Engineering Sciences, University of Colorado at Boulder, Boulder, Colorado, USA

This article presents a unified model for the velocity of discrete microdroplets. Simple algebraic expressions for steady-state droplet velocities are presented, as well as exact and approximate transient solutions. Specific results in terms of known experimental parameters are derived for the cases of electrowetting on dielectric (EWOD), dielectrophoresis (DEP), continuous electrowetting (CEW), and thermocapillary pumping (TCP). Model predictions are shown to agree with previously published theoretical and experimental results, giving fluid velocities for a broad range of applications in digitized microfluidics. A relative comparison of the model's predictions for EWOD, CEW, DEP and TCP is also presented.

KEY WORDS: digital microfluidics, electrowetting on dielectric, dielectrophoresis, droplet transport

INTRODUCTION

As advances in fabrication lead to smaller and smaller device sizes, new methods for microscale fluid control are being developed. The growing field of digital microfluidics, in which discrete droplets are manipulated in place of continuous flows, has allowed for the fabrication of compact, efficient and highly programmable microfluidic devices [1–12]. When individual droplets are used, fixed volumes of liquid may be precisely manipulated on a fabricated grid of electrodes; this reduces the required amount of fluid and increases the degree of control, leading to less cross-contamination, lower actuation voltages, and lower power consumption.

Several actuation forces with scaling relationships conducive to microscale flows are currently under research. These include electrostatic stresses as well as direct modulation of surface tension by chemical, optical, or thermal means. This paper presents a simplified model for the velocity of microdroplets actuated by any of the above methods in 2D planar geometry. Steady-state and transient results are first derived for a general force per unit width applied to a droplet; specific results for electrowetting on dielectric (EWOD), continuous electrowetting (CEW), dielectrophoresis, and thermocapillary pumping (TCP) are then presented. Predictions of the model are shown to be in exact agreement with previously

The authors would like to acknowledge partial support by AFOSR Contract No. FA9550-05-1-0334 and NSF Contract No. CTS-0540004.

Address correspondence to K. Mohseni, Aerospace Engineering Sciences, University of Colorado at Boulder, 111 Engineering Drive, Engineering Center Room ECAE 197, Boulder, CO 80309-0429. E-mail: mohseni@colorado.edu

NOMENCLATURE

A	area of fluid in contact with channel wall	u_{SS}^{avg}	y-averaged steady state velocity
C	capacitance	u_H^{avg}	y-averaged steady state velocity including hysteresis
c	capacitance per unit area	V	applied voltage
E	energy per area	w	width of droplet
F	net force	x	axial coordinate
H	hysteresis force	y	transverse coordinate
h	channel height	Greek Symbols	
K	kernel of diffusion equation	ϵ_0	vacuum dielectric constant
L	droplet Length	ϵ	dielectric constant of channel coating
m	mass	μ	viscosity
t	time coordinate	ρ	density
U	electrostatic energy	τ	time scale
u	velocity		
u^{avg}	y-averaged velocity		

published empirical and analytical results for CEW and TCP. Finally, a relative comparison of these four actuation methods for application in microfluidic devices is presented.

THEORETICAL MODEL

We consider a microchannel of height h and width w containing a fluid droplet of length L , viscosity μ , and density ρ , as seen in Figure 1. For simplicity we assume $w \gg h$, such that the flow can be considered two-dimensional and there is no z dependence. Any actuation force F , regardless of its distribution on the droplet interfaces, is modeled as an equivalent pressure gradient for substitution into the Navier-Stokes equation:

$$\frac{dp}{dx} = \frac{\Delta P}{L} = \frac{Fhw}{L} \quad (1)$$

We assume laminar, unidirectional flow such that the fluid velocity is given by $u = u(y,t)$. Numerical results from a modified cavity solver in our group indicate this is a valid assumption except near the droplet interfaces when L is several times larger than h . Under this assumption, the nonlinear term in the one-dimensional Navier-Stokes equation vanishes, and the equation reduces to:

$$\rho \frac{\partial u}{\partial t} = \frac{-\Delta P}{L} + \mu \frac{\partial^2 u}{\partial y^2} \quad (2)$$

We apply no-slip boundary conditions along the top and bottom walls. The droplet is able to translate while simultaneously satisfying the no-slip condition through a rolling motion: Torques produced by viscous drag along the channel walls induce twin vortices in the droplet of equal magnitude but opposite sign. As the droplet itself moves forward, internal circulation at the front and rear interface ensures that the fluid adjacent to the top and bottom walls is stationary at all times. This internal circulation has been observed in Paik et al. [13].

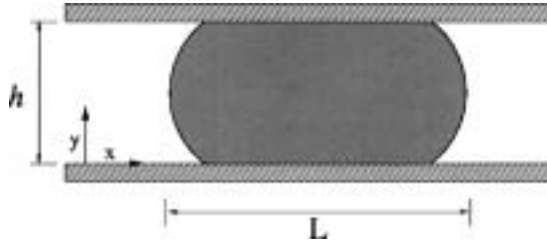


Figure 1. Droplet in channel.

Steady-State Velocity

The steady-state velocity of the droplet is obtained by setting $\partial/\partial t = 0$ in Eq. (3):

$$\frac{\Delta P}{L} = \mu \frac{\partial^2 u}{\partial^2 y} \tag{3}$$

Equation (4) directly expresses the balance of the driving force and viscous drag at steady-state. The equation is readily integrated twice, giving:

$$u_{ss}(y) = 6u_{ss}^{avg} \left(\frac{y}{h} - \frac{y^2}{h^2} \right) \tag{4}$$

where u_{ss} is the steady-state velocity of the droplet and u_{ss}^{avg} is the y -averaged velocity of the droplet, is given by:

$$u_{ss}^{avg} = \frac{h^2}{12\mu} \frac{\Delta P}{L} \tag{5}$$

which is the standard result for the average velocity of Poiseuille flow between parallel plates [14]. Rather than representing the average velocity of a continuous channel flow, however, Eq. (5) now gives the bulk velocity of a discrete translating droplet.

Exact Transient Velocity

To obtain a transient solution to the full Navier-Stokes equation we nondimensionalize the y coordinate with the characteristic length scale, h . After making the substitution $\bar{y} = y/h$ and rearranging, Eq. (3) becomes

$$\frac{\rho h^2}{\mu} \frac{\partial u}{\partial t} = \frac{\partial^2 u}{\partial \bar{y}^2} - \frac{\Delta P}{L} \tag{6}$$

The form of Eq. (6) suggests nondimensionalizing the time coordinate via the substitution $\bar{t} = \mu t / \rho h^2$. The nondimensionalized Navier-Stokes equation then reads

$$\frac{\partial u}{\partial \bar{t}} = \frac{\partial^2 u}{\partial \bar{y}^2} - \frac{h^2 \Delta P}{\mu L} \tag{7}$$

This is a diffusion equation in standard form. The exact solution of Eq. (7) under the boundary conditions of $u = 0$ at $\bar{y} = 0$ and $\bar{y} = 1$, as well as the initial condition $u = 0$ for $\bar{t} = 0$, is given in Cannon [15] as:

$$u(\bar{y}, \bar{t}) = \frac{h^2 \Delta P}{8\mu L} \int_0^{\bar{t}} \int_0^1 [\Theta(\bar{y} - \xi, \bar{t} - \gamma) - \Theta(\bar{y} + \xi, \bar{t} - \gamma)] d\xi d\gamma \quad (8)$$

where

$$\Theta(x, t) = \sum_{m=-\infty}^{m=+\infty} K(x + 2m, t) \quad (9)$$

and K is the fundamental solution of the one-dimensional diffusion equation, given by:

$$K(x, t) = \frac{1}{\sqrt{4\pi t}} \exp\left(-\frac{x^2}{4t}\right) \quad (10)$$

Plots of this solution at several values of time are given in Figure 2. For very short times, the velocity profile is flat near the middle and steep at the top and bottom; towards the center of the droplet, the effect of viscous drag at the walls has not yet had time to appear and the droplet moves as a rigid body. As time progresses, the profile becomes parabolic and the droplet continues accelerating. For long times, the velocity profile exactly approaches the steady-state result obtained in the previous section.

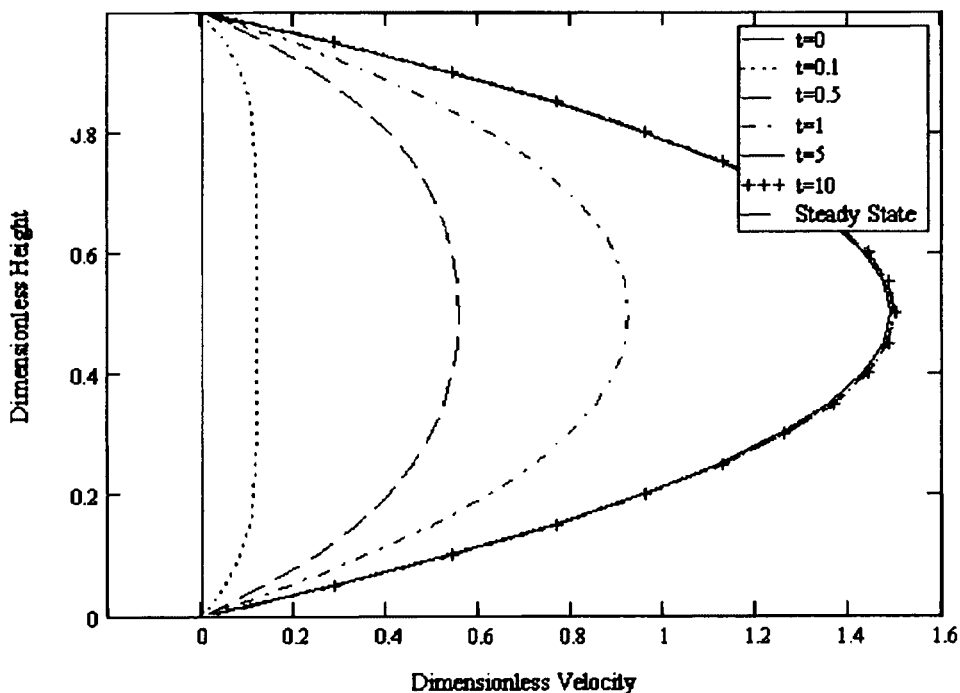


Figure 2. Velocity profile for several values of t/τ . The y axis is $y = y/h$, the x axis is $u(\bar{y}, \bar{t})/u_{avg}^{ss}$. The profile is originally flat toward the center as the effect of viscous drag at the walls diffuses into the droplet. As the droplet is accelerated, the profile takes on a parabolic shape and eventually matches the steady state result given by Eqs. (4) and (5).

Transient Velocity with Parabolic Profile

In Yang et al. [16], the position of the meniscus of an advancing column of fluid is found by substituting a parabolic velocity profile into the Navier-Stokes equation before solving. Figure 2 suggests that the assumption of a parabolic profile is approximately valid for an accelerating droplet at times greater than $\bar{t} = \rho h^2 / \mu$. A numerical simulation performed in Mohseni et al. [17] with a slip length treatment of contact line singularity also returns an approximately parabolic velocity profile, as seen in Figure 3.

Substituting a parabolic profile into the Navier-Stokes equation and solving gives a simple algebraic expression for an approximate transient solution. For long times, both the approximate and exact solutions match the steady-state velocity derived previously. We assume the droplet's velocity can be written as:

$$u(y, t) = 6u^{avg}(t) \left(\frac{y}{h} - \frac{y^2}{h^2} \right) \quad (11)$$

which automatically satisfies a no-slip boundary condition along the top and bottom walls of the microchannel. $u^{avg}(t)$ is the average velocity of the droplet as a function of time.

When this velocity profile is substituted into the Navier-Stokes equation and averaged over the y direction, the equation reduces to a simple ordinary differential equation in time:

$$\frac{du(t)}{dt} + \frac{12\mu}{\rho h^2} u(t) = \frac{3\Delta P}{2\rho L} \quad (12)$$

The form of Eq. (12) suggests that the natural time scale of this equation is given by:

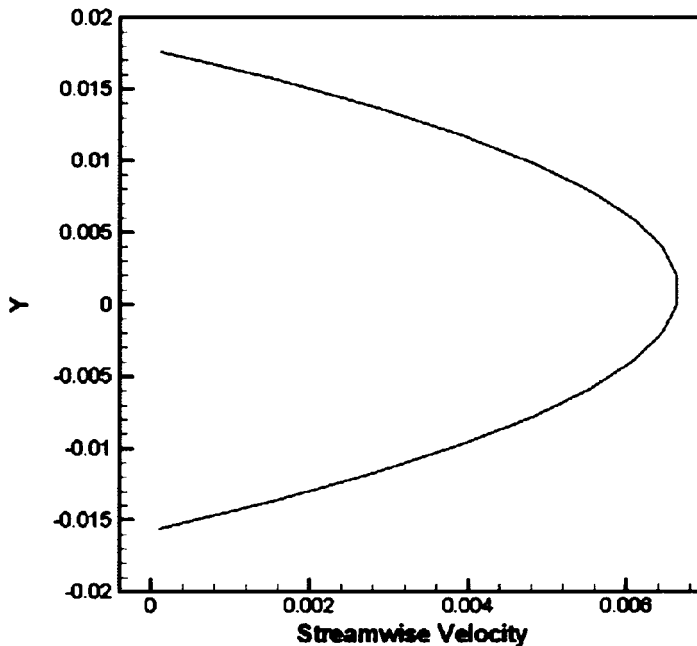


Figure 3. Numerical velocity profile given by applying a slip-length condition at the contact line for an advancing droplet.

$$\tau = \frac{\rho h^2}{12\mu} \quad (13)$$

The solution to Eq. (12) is readily seen to be

$$u(t) = u_{ss}^{avg} \left(1 - e^{-t/\tau} \right) \quad (14)$$

with u_{ss}^{avg} defined as previously.

A plot comparing the exact transient solution with the approximate transient solution at several different values of t/τ is given in Figure 4. As seen in the figure, the parabolic solution is a fair approximation even at small times and exactly matches the exact solution for $t \gg \tau$. The time scaling present in the approximate solution, τ , is seen to be the ratio of the droplet's steady-state momentum to the driving force.

Other Forces

Additional drag forces such as wind resistance and contact line friction may be added to this simplified model. The effect of wind resistance due to air is expected to be negligible as its viscosity is significantly lower than the fluid's. Contact line friction, a velocity-dependent drag force acting on an advancing contact line, is a new topic of research. Introducing this force into the Navier-Stokes equation changes the scaling of the final result, however. Experimental data in Pollack et al. [2] suggest the scaling of Eq. (5) (with ΔP derived from the EWOD force) holds over a large range of velocities. In addition, analytical results derived without contact line friction were found to be in agreement with empirical data in Yang et al. [16]. The effect of contact angle *hysteresis*, however, is important when dealing with discrete droplets. This effect is added to the model below.

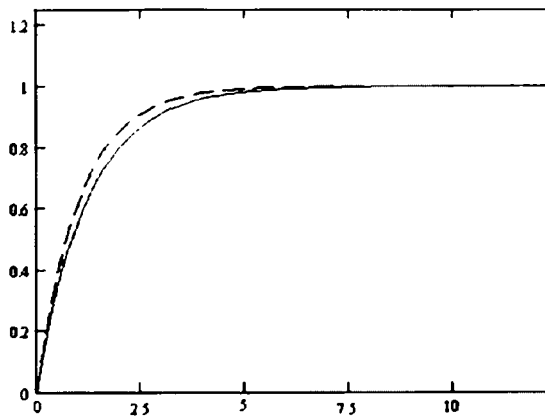


Figure 4. Average velocity of an EWOD-actuated microdroplet as a function of time. The y axis is $y = y/h$, the x axis is $\bar{t} = t/\tau = t/\tau$. Solid line is exact solution given by averaging Eq. (9) over the y coordinate, dashed line is approximate solution given by Eq. (14).

STEADY VELOCITIES FOR 2D FLOWS

In this section, specific results will be derived from Eq. (5) by substituting in a specific formula for ΔP . In EWOD, DEP, and CEW, ΔP will be derived from a capacitive energy; for TCP, ΔP will be a thermally induced difference in surface tension. Results will be given for a parallel plate geometries for each actuation method.

Electrowetting on Dielectric

In electrowetting on dielectric, a microchannel is lined with a thin layer of electrically insulating material, as seen in Figure 5, and a voltage is applied across the height of the channel. The total energy of the system can be expressed via the usual formula for the energy stored in a capacitor:

$$U = \frac{1}{2} CV^2 \tag{15}$$

where C is the net capacitance of the dielectric coatings and V is the applied voltage. The energy in regions of empty channel is negligibly small in the limit of $d \ll h$, which is usually the case for an EWOD device. The EWOD force is generated by lining a channel with electrodes and sequentially firing them such that the leading edge is continually between a charged electrode and ground, whereas the trailing edge is always between grounded electrodes. In this case, the area of the charged capacitor is $A = xw$, where w is the channel width and x is the length of droplet between charged electrodes. The total force on the conductor in any direction can be found by simply differentiating the total energy of the system at fixed potential with respect to the coordinate variable [18–20]:

$$F = \frac{\partial U}{\partial x} \tag{16}$$

When one side of the channel is lined with a continuous, uninsulated grounding electrode, the droplet is grounded and the total force is directly given by Eqs. (16) and (17),

$$\Delta P = \frac{F}{wh} = \frac{1}{wh} \frac{\partial U}{\partial x} = \frac{1}{2h} cV^2 \tag{17}$$

where c is the capacitance per area of the dielectric layers. Eq. (18) is the equivalent pressure gradient drawing the droplet into the region of applied field. This gives a steady-state velocity of

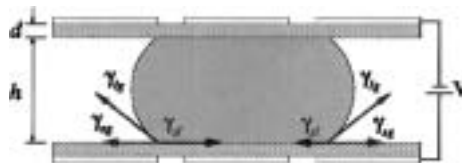


Figure 5. EWOD configuration.

$$u_{ss}^{avg} = \frac{cV^2 h}{24\mu L} \quad (18)$$

The scaling of this force is exactly the same as that of surface tension; that is, the net force is directly proportional to the width of the droplet's contact line, and is completely independent of the droplet's height or length. For this reason, EWOD dominates actuation methods which scale with the fluid's area or volume, such as pressure or body forces, at sufficiently small length scales. Note that the EWOD force does not depend on fluid properties such as surface tension or contact angle; the only assumption is that the fluid is considered perfectly conducting.

Continuous Electrowetting

In continuous electrowetting, a droplet of liquid metal is suspended in an electrolyte solution, as shown in Figure 6. A difference in surface tension is again created between the front and rear of the droplet through the application of an electric field, this time along the direction of flow. Resistance in the electrolytic fluid creates a potential gradient in the electrolyte between the front and rear of the droplet. This creates a difference in energy stored in the EDL. The difference in surface energy between the front and rear of the droplet is given by

$$\Delta E = q\Delta\varphi \quad (19)$$

Here, q is the average charge per unit area present on the droplet before a field is applied and $\Delta\varphi$ is the difference in electric potential between the front and rear of the droplet. This potential difference is due to the large resistance of the thin layer of fluid between the droplet and wall.

Substituting Eq. (20) into Eq. (17) to find ΔP and subsequently using Eq. (6) gives a formula for the steady-state velocity of a droplet actuated by CEW:

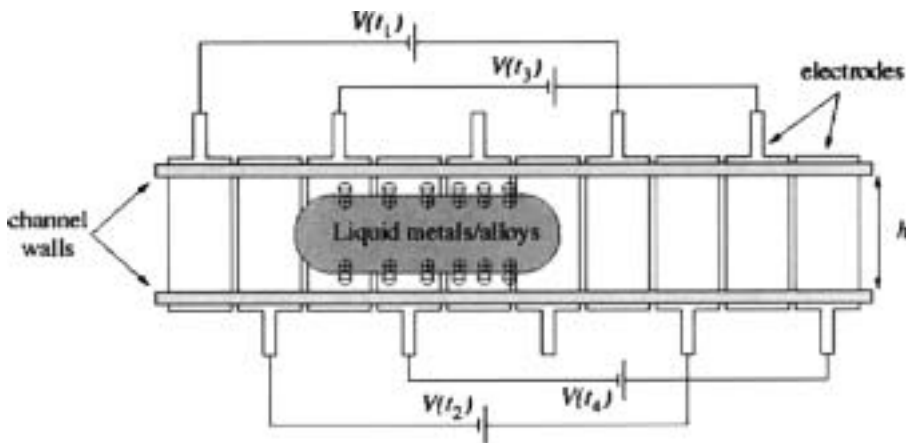


Figure 6. CEW configuration.

$$\frac{q\Delta\varphi h}{6\mu L} \quad (20)$$

This matches the results of Jackel *et al.* [21]. Similar to EWOD actuation, the steady state velocity for a droplet actuated by CEW is essentially independent of size, depending only on the droplet's height-to-length ratio.

Dielectrophoresis

In dielectrophoresis, an insulating fluid is used for the droplet, and the channel is not necessarily isolated with a dielectric coating. DEP arises from a slightly different physical mechanism. Here, a force acts all along the front face of the droplet as a consequence of the nonlinear fringing field along the edge of the charged electrodes. The result of Eq. (17) is simply the difference between a dielectric-filled capacitor and an empty one [18–20]. The steady-state velocity is rapidly found to be

$$\frac{(\epsilon - \epsilon_0)}{12\mu L} V^2 \quad (21)$$

where ϵ is now the dielectric constant of the fluid itself and ϵ_0 is the vacuum dielectric. Note that dielectrophoresis has a different scaling. Now, instead of depending on h/L , the velocity depends only on $1/L$, making dielectrophoresis increasingly effective for very small channel sizes.

Thermocapillary Pumping

In thermocapillary motion, the liquid–gas surface tension itself is directly modified through the application of a temperature gradient [22]. If the surface tension is assumed to vary linearly with temperature,

$$\gamma_{st} = a - bT \quad (22)$$

where T is the temperature and a and b are experimentally defined constants, the x component of force on the droplet is given by:

$$w \left(\frac{d\gamma_{st}}{dT} \Delta T \right) \cos(\theta) = -bw\Delta T \cos(\theta) \quad (23)$$

Note that the actual values of the equilibrium contact angle and surface tension do play a role in TCP. This force, per width, results in a steady-state velocity of

$$\frac{-b\Delta T \cos(\theta)h}{6\mu L} \quad (24)$$

Contact Angle Hysteresis

The above derivations neglect the effects of contact angle hysteresis on EWOD, DEP, and TCP. When a droplet moves along a surface, the front (advancing) and rear (receding) contact angles each differ from the equilibrium value. As a force is applied to an initially stationary droplet and gradually increased from zero, no motion is observed below a certain threshold as the front and rear contact angles change to exactly balance out the applied stress. Above this threshold, the contact angles cease

changing and the droplet begins to translate. While several mechanisms for contact angle hysteresis, including chemical heterogeneity, surface roughness, charge trapping, and others have been studied, there is currently no rigorous formula for calculating the hysteresis angles [23, 24]. The advancing and receding angles must therefore be determined empirically by tilted plate measurements or other means [24]. Contact angle hysteresis may be added to our model if measured values for the advancing and retreating angles are known. For simplicity, we consider hysteresis only in steady state and neglect transient effects such as the dynamics of contact line friction and the possible velocity dependence of the advancing and retreating angles.

Contact angle hysteresis may be added to the model for EWOD and DEP if the advancing and retreating angles are known. With unequal contact angles, a hysteresis force H , is given by the difference in the axial component of surface tension at the front and rear of the droplet:

$$H = w\gamma_{sl}[\cos(\theta_a) - \cos(\theta_r)] \quad (25)$$

where a and r stand for advancing and receding. When the driving force is below this hysteresis force, no motion is obtained and the droplet remains stationary. For EWOD, this results in a threshold voltage given by:

$$V_{thresh}^2 = \frac{8H}{c} \quad (26)$$

and a modified steady-state velocity of

$$u_H^{avg} = \frac{c(V^2 - V_{thresh}^2)h}{24\mu L} \quad (27)$$

above the threshold voltage, where u_H^{avg} represents the average, steady-state droplet velocity with contact angle hysteresis taken into account. The same threshold voltage is likewise inserted into the velocity for DEP-actuated microdroplets.

The effect of contact angle hysteresis on thermocapillarity is more subtle; this is because the liquid–gas surface tension itself is being directly modified, and the separate advancing and receding contact angles must be used in Eq. (24). After combining equations and rearranging, the final velocity for TCP-actuated droplets is derived:

$$w\left(\frac{d\gamma_{sl}}{dT}\Delta T\right)\cos(\theta) = -bw\Delta T\cos(\theta) \quad (28)$$

This is the same result given by a different derivation in Richter et al. [25] and Sammarco and Burns [26]. A plot of Eq. (29) with experimental data obtained in Chen et al. [24] is given in Figure 7. A comparison table of actuation methods is given in Table 1.

CONCLUSIONS

This article predicts the velocity of discrete droplets propelled across solid surfaces by electrostatic or surface tension stresses. These stresses are controlled through the application of an electric field or thermal gradient, and have very favorable scaling relationships for use in microscale. The model presented, while very simple, provides useful expressions for the transient and steady-state velocities of a microdroplet and is easily generalized to any method

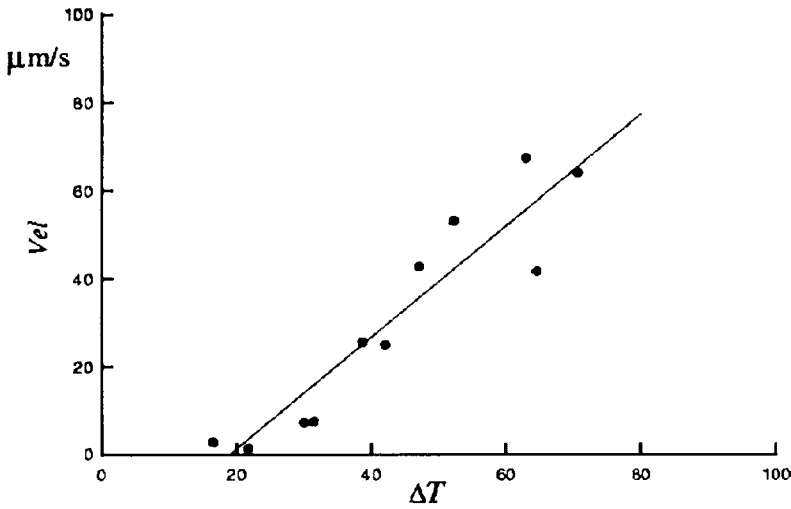


Figure 7. Velocity of a TCP actuated droplet: Eq. (29) (solid line) and experimental data (points).

Table 1 Actuation forces and steady-state velocities for digital microfluidics

Method	Force per length	2-D plane velocity
EWOD	$\frac{c_{layer}(V^2 - V_{thresh}^2)}{8d}$	$\frac{c_{layer}(V^2 - V_{thresh}^2)h}{48\mu d L}$
CEW	$q\Delta\phi$	$\frac{q\Delta\phi h}{6\mu l}$
DEP	$\frac{1}{2} \frac{\epsilon - \epsilon_0}{h} (V^2 - V_{thresh}^2)$	$(\epsilon - \epsilon_0) \frac{(V^2 - V_{thresh}^2)}{12\mu L}$
TCP	$\left(\frac{d\gamma_{sl}}{dT} \frac{dT}{dL}\right) \cos(\theta)$	$\frac{hb \cos(\theta_r)}{6L\mu} \left[\Delta T + \left(T_a - \frac{a}{b}\right) \left(1 - \frac{\cos(\theta_a)}{\cos(\theta_b)}\right) \right]$

of actuation. These expressions provide a direct and efficient method for estimating droplet velocities for applications across the field of digital microfluidics.

REFERENCES

1. M.G. Pollack, R.B. Fair, and A.D. Shenderov, Electrowetting-Based Actuation of Liquid Droplets for Microfluidic Applications, *Applied Physics Letters*, Vol. 77(11), pp. 1725–1726, 2000.
2. M.G. Pollack, R.B. Fair, and A.D. Shenderov, Electrowetting-Based Actuation of Droplets for Integrated Microfluidics, *Lab on a Chip*, Vol. 2(2), pp. 96–101, 2002.
3. E. Colgate and H. Matsumoto, An Investigation of Electrowetting-Based Microactuation, *Journal of Vacuum Science and Technology A*, Vol. 8(4), pp. 3625–3623, 1990.

4. F. Mugele and J.C. Baret. Electrowetting: From Basics to Applications, *Journal of Physics: Condensed Matter*, Vol. 17(28), pp. R705–R774, 2005.
5. V. Srinivasan, V.K. Pamula, M.G. Pollack, and R.B. Fair, Clinical Diagnostics on Human Whole Blood, Plasma, Serum, Urine, Saliva, Sweat, and Tears on a Digital Microfluidic Platform, Duke University, Durham, NC, 2003.
6. R.B. Fair, A. Khlystov, V. Srinivasan, V.K. Pamula, and K.N. Weaver, Integrated Chemical/Biochemical Sample Collection, Pre-concentration, and Analysis on a Digital Microfluidic Lab-on-a-Chip Platform, Lab-on-a-Chip: Platforms, Devices, and Applications, Conf. 5591, SPIE Optics East, Philadelphia, Oct. 25–28, 2004.
7. B. Shapiro, H. Moon, R.L. Garrell, and C.J. Kim, Equilibrium Behavior of Sessile Drops under Surface Tension, Applied External Fields, and Material Variations, *Journal of Applied Physics*, Vol. 93(9), pp. 5794–5811, 2003.
8. J. Lee, H. Moon, J. Fowler, T. Schoellhammer, and C.J. Kim, Electrowetting and Electrowetting-on-Dielectric for Microscale Liquid Handling, *Sensors and Actuators A: Physical*, Vol. 95, pp. 259–268, 2002.
9. J. Lee and C.J. Kim, Surface-Tension-Driven Actuation Based on Continuous Electrowetting, *J. MEMS*, Vol. 9(2), pp. 220–225, 2000.
10. S.K. Cho, H. Moon, and C.J. Kim, Creating, Transporting, Cutting, and Merging Liquid Droplets by Electrowetting-Based Actuation for Digital Microfluidic Circuits, *Journal of Microelectromechanical Systems*, Vol. 12(1), pp. 70–80, 2003.
11. T. Jones, J. Fowler, Y. Chang, and C. Kim, Frequency-Based Relationship of Electrowetting and Dielectrophoretic Liquid Microactuation, *Langmuir*, Vol. 19, pp. 7646–7651, 2003.
12. T. Jones and K. Wang, Frequency-Dependent Electromechanics of Aqueous Liquids: Electrowetting and Dielectrophoresis, *Langmuir*, Vol. 20, pp. 2813–2818, 2004.
13. P. Paik, V. Pamula, and R. Fair, Rapid Droplet Mixers for Digital Microfluidic Systems, *Lab on a Chip*, Vol. 3, pp. 253–259, 2003.
14. D. Tritton, *Physical Fluid Dynamics*, Oxford Science Publications, New York, 1977.
15. J. Cannon, *The One-Dimensional Heat Equation*, Addison-Wesley Pub. Co, Boston, 1984.
16. L. Yang, T. Yao, Y. Huang, Y. Xu, and Y. Tai, The Marching Velocity of the Capillary Meniscus in Microchannels, *Journal of Micromechanics and Microengineering*, Vol. 14, pp. 220–225, 2004.
17. K. Mohseni, H. Zhao, and E. Baird, Digitized Heat Transfer for Thermal Management of Compact Systems, IMECE 2005–79372, Orlando, FL, November 2005.
18. D. Griffiths, *Introduction to Electrodynamics*, Prentice Hall, New York, 1999.
19. L. Landau and E. Lifshitz, *Electrodynamics of Continuous Media*, Pergamon Press, Englewood Cliffs, NJ, 1960.
20. J. Jackson, *Classical Electrodynamics*, 3rd Ed., John Wiley and Sons, Inc., New York, 1999.
21. J.L. Jackel, S. Hackwood, J. Veselka, and G. Beni, Electrowetting Switch for Multimode Optical Fibers, *Applied Optics*, Vol. 22, pp. 1765–1770, 1983.
22. T. Sammarco and M. Burns, Thermocapillary Pumping of Discrete Drops in Microfabricated Devices, *AIChE Journal*, Vol. 45, pp. 350–366, 1999.
23. V. Dussan and R. Chow, On the Ability of Drops or Bubbles to Stick to Non-Horizontal Surfaces of Solids, *Journal of Fluid Mechanics*, Vol. 137, pp. 1–29, 1983.
24. J.Z. Chen, S.M. Troian, A.A. Darhuber, and S. Wagner. Effect of Contact Angle Hysteresis on Thermocapillary Droplet Actuation, *Journal of Applied Physics*, Vol. 97(014906), pp. 1–9, 2005.
25. M. Richter, P. Woias, and D. Weiss, Microchannel for Applications in Liquid Dosing and for Rate Measurement, *Sensors and Actuators A*, Vol. 62, p. 480, 1997.
26. T. Sammarco and M. Burns, Heat Transfer Analysis of Microfabricated Thermocapillary Pumping and Reaction Devices, *Journal of Micromechanics and Microengineering*, Vol. 10, pp. 42–55, 2000.